Nanoscale

PAPER

View Article Online
View Journal

Cite this: DOI: 10.1039/c7nr00227k

Rational design of super-alkalis and their role in CO_2 activation†

Tianshan Zhao,[a,b] Qian Wang*[a] and Puru Jena*[b]

Received 10th January 2017,
Accepted 8th February 2017

DOI: 10.1039/c7nr00227k

rsc.li/nanoscale

Super-alkalis are clusters of atoms. With ionization potentials smaller than those of the alkali atoms, they are playing an increasing role in chemistry as highlighted by recent applications in solar cells as well as in Li-ion batteries. For the past 40 years superalkalis were designed using inorganic elements with the sp orbital character. Here, we show that a large class of superalkalis composed of only simple metal atoms, transition metal complexes as well as organic molecules can be designed by making use of electron counting rules beyond the octet rule. Examples include Al_3^+, $Mn(B_3N_3H_6)_2^+$, $B_9C_3H_{12}^+$, and $C_5NH_6^+$ which obey the jellium shell closure rule, the 18-electron rule, the Wade–Mingos rule, and Hückel's aromatic rule, respectively. We further show that the ability of superalkalis to transfer an electron easily can be used to activate a CO_2 molecule by transforming it from a linear to a bent structure. These results, based on density functional theory with generalized gradient approximation for exchange–correlation potential, open the door to a new class of catalysts for CO_2 activation.

Introduction

Atomic clusters possess unique properties that depend on their size and composition and can be designed to mimic the chemistry of atoms in the periodic table. Such clusters, known as "superatoms"[1,2] can then be used as the building blocks of a new three-dimensional periodic table. Superalkalis and superhalogens belong to a special class of superatoms that mimic the chemistry of alkali and halogen atoms, respectively. In the early 1980s Gutsev and Boldyrev designed these super-alkalis[3] and super-halogens[4] by using sp elements. An example of a super-alkali cluster is M_2X while that of a super-halogen is MX_2 (M = Li, Na, K, Rb, Cs; X = F, Cl, Br, I). The former contains one electron more while the latter contains one electron less than needed for octet-shell closure. Consequently, the ionization potential of M_2X is smaller than that of M and the electron affinity of the latter is larger than that of X, hence the name super-alkalis and super-halogens. There has been considerable interest in discovering super-alkalis and superhalogens as they, respectively, act as reducing and oxidizing agents.

Most of the early efforts in superhalogens were confined to simple metals (such as alkalis, Mg, and Al) decorated with halogens. The list of superhalogens has expanded greatly in the last decade as it was shown that they can be designed by using other electron counting rules such as the 18-electron rule,[5] Wade–Mingos rule,[6] and aromatic rule.[7] Superhalogens composed of only transition metals,[5] transition metals and oxygen,[8] as well as compositions that do not include a single metal or halogen atom[5] are now known. The role of super-halogens as the building block of electrolytes in metal-ion batteries,[9,10] hybrid perovskite solar cells,[10] light emitting diodes,[11] as well as hydrogen storage materials[12] has further heightened their relevance in materials design.[13]

While nonmetallic as well as poly-nuclear superalkali cations with various functional groups as the central core have been studied,[14] no attempts have been made,[14,15] similar to those of superhalogens, to synthesize superalkalis using different electron counting rules. In this paper, we use the jellium rule, the 18-electron rule, the Wade–Mingos rule, and Hückel's aromatic rule to design superalkalis and examine their role in the activation of a CO_2 molecule. The results are compared with the activation of CO_2 using coinage metal atoms.

Results and discussion

Rational design of super-alkalis

Typical examples of superalkalis that have been studied earlier are Li_3O, Cs_2Cl, and Cs_2NO_3.[16,17] These moieties, analogous to

[a]Center for Applied Physics and Technology, College of Engineering, Peking University, Key Laboratory of High Energy Density Physics Simulation, and IFSA Collaborative Innovation Center, Ministry of Education, Beijing 100871, China. E-mail: qianwang2@pku.edu.cn
[b]Department of Physics, Virginia Commonwealth University, Richmond, VA 23284, USA. E-mail: pjena@vcu.edu

†Electronic supplementary information (ESI) available. See DOI: 10.1039/c7nr00227k

those of alkali atoms, contain one extra electron than needed for the octet shell closure. The ionization potentials of these clusters, namely, 3.85 eV, 3.00 eV, and 3.12 eV (ref. 16) are smaller than those of alkali atoms (5.39, 5.14, 4.34, 4.18, and 3.89 eV for Li, Na, K, Rb, and Cs, respectively). In the following we discuss how other electron counting rules that have been used to describe the stability of superhalogens can also be used to design superalkalis.

Jellium rule. The jellium model was introduced by Knight and coworkers to explain the pronounced stability of Na_n clusters containing 2, 8, 20, 40, ... atoms. In this model a cluster is replaced by a sphere of uniform distribution of positive charge and the corresponding electronic energy levels and total energy are calculated. Because of the spherical symmetry of the potential, the electronic energy levels are arranged in $1s^2 1p^6 1d^{10} 2s^2 1f^{14}$... shells. As each successive shell is filled, the corresponding cluster exhibits enhanced stability. Thus, Na_n clusters containing 2, 8, 20, 40, ... atoms are more stable than their neighbors. A cluster containing 39 electrons would then need an extra electron for jellium shell closure just like a halogen atom with 7 electrons would require one extra electron to complete the s^2p^6 octet shell closure. Thus, Al_{13} would behave like a halogen atom. The measured electron affinity of 3.6 eV of Al_{13} indeed confirmed[18] this expectation.

By the same token, consider the Al_3 cluster. Earlier studies have shown that Al in small clusters containing 7 or fewer number of atoms behaves as a monovalent species,[18,19] Al_3 would then have 3 valence electrons, one more than that needed for the electron shell closure, just as is the case with alkali atoms. Thus, one would expect Al_3 to behave as an alkali atom and if its ionization potential is less than that of an alkali atom, it could be termed a super-alkali. The situation would still be the same even if Al is considered to be trivalent in small clusters. Al_3 would then contain 9 electrons, one more than needed for jellium shell closure. The computed geometry of Al_3^+ is a planar triangle with a C_{3v} symmetry and Al–Al bond length of 2.68 Å (see Fig. 1). This compares well with the previous result of 2.83 Å (ref. 19) computed at the MP2 level of theory. The ionization potential calculated by taking the energy difference between the ground state of the neutral and the cation at the neutral geometry is 4.75 eV (see Table 1). This is less than the ionization potential of the Na atom and confirms that superalkalis can be constructed from free-electron metals by using the jellium shell closure rule. To study the thermal stability of the Al_3^+ super-alkali at finite temperature, we performed *ab initio* molecular dynamics (AIMD) simulations at 400 K. The time step was set as 1 femtosecond (fs). After 10 picoseconds of simulation, no structural distortion or reconstruction was found, and the average total potential energy remained nearly constant as shown in Fig. S1a,† confirming that Al_3^+ is thermally stable at room temperature. With regard to the simulated infrared (IR) spectroscopy, we found that the vibrational frequencies of Al_3^+ are mainly distributed in the 200 to 250 cm^{-1} region; in the Raman spectroscopy, the peak distribution is around 270 cm^{-1}. These results are given in Fig. S2a.†

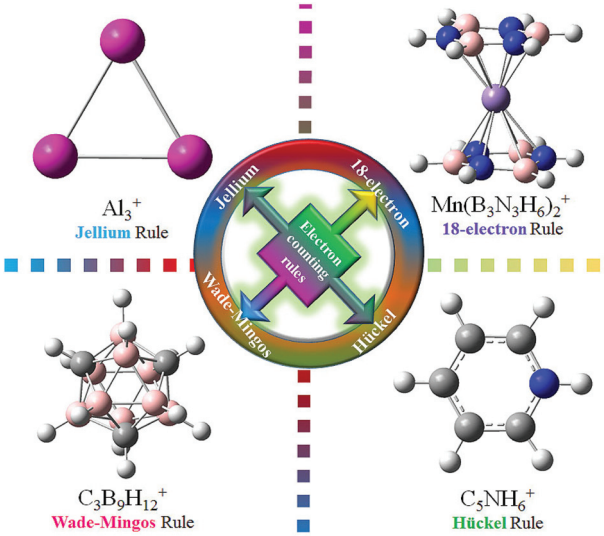

Fig. 1 Optimized geometries of four different kinds of superalkalis. Legends are cation's name and electron counting rules applied.

Table 1 Molecular volume, ionization potential (IP), O–C–O bond angle, average C–O bond length, NBO charges transferred to CO_2, and the HOMO–LUMO gap of superalkali cations. Results are compared with CO_2 interacting with Cu, Ag, and Au[20]

Cations	Volume ($cm^3\ mol^{-1}$)	IP (eV)	Angle (°)	C–O bond (Å)	NBO charge transfer (e)	Gap (eV)
Al_3	72.79	4.75	126	1.40	1.26	4.97
$B_9C_3H_{12}$	126.83	3.64	131	1.29	0.91	14.77
C_5NH_6	64.41	3.95	129	1.35	0.63	11.65
$Mn(B_3N_3H_6)_2$	127.10	4.35	133	1.25	0.90	6.79
CO_2^- (anion)			137	1.24	1	
Cu	—	7.73	139	1.22	0.64	—
Ag	—	7.58	173.5	1.16	—	—
Au	—	9.23	145	1.20	0.45	—

From an analysis of the frontier molecular orbitals (FMOs) of a neutral Al_3 cluster shown in Fig. S3a† we find that the highest occupied molecular orbital (HOMO) is mainly contributed by aluminum $3p_z$ orbitals. The lowest unoccupied molecular orbital (LUMO) mainly exhibits σ bonding. The HOMO–LUMO gap is estimated to be 4.97 eV, which also confirms the unusual stability of the cation in the gas phase. To be specific, the electron configuration of each Al atom in Al_3^+ is $3s^{1.68}3p^{0.97}$, which means that aluminum loses 0.32 s orbital electrons per atom. This is a simple example of how the jellium shell closure rule can be used to design superalkalis. In the later part of the section we will discuss the role Al_3^+ can play in CO_2 activation.

We also considered a hetero-atomic cluster $Al_{12}N$ which has $12 \times 3 + 5 = 41$ electrons, one electron more than needed for the jellium shell closure. The calculated ionization potential of $Al_{12}N$ is 4.81 eV which confirms that it too is a superalkali.

18-Electron rule. This rule generally applies to complexes containing transition metal atoms which require 18 electrons

to fill the $s^2p^6d^{10}$ orbitals. Classic examples of a stable compound obeying the 18-electron rule are ferrocene, $Fe(C_5H_5)_2$, where the Fe atom is sandwiched between two C_5H_5 molecules and chromium bis-benzene, $Cr(C_6H_6)_2$, where the Cr atom is sandwiched between two benzene molecules. With the $3d^64s^2$ ($3d^54s^1$) electronic configuration of the Fe (Cr) atom and 5 (6) π-electrons coming from each of the C_5H_5 (C_6H_6) molecules, $Fe(C_5H_5)_2$ and $Cr(C_6H_6)_2$ contain 18-electrons each which account for their unusual stability. Similarly, it was predicted[21] and later experimentally verified[22] that $Au_{12}W$ with 18 electrons is unusually stable and $Au_{12}Ta$, which contains one less electron than required by the 18-electron rule, has an electron affinity of 3.65 eV,[5] thus behaving as a superhalogen. We explored if the 18-electron rule can be successfully used to design a superalkali.

Here we show that the $Mn(B_3N_3H_6)_2^+$ cation which is isoelectronic with $Cr(C_6H_6)_2$ [23] is very stable and neutral $Mn(B_3N_3H_6)_2$ which contains one electron more than needed to satisfy the 18-electron rule is a superalkali. We optimized the geometry of $Mn(B_3N_3H_6)_2$ by starting with different configurations as given in the ESI.† The ground state geometry is that of the Mn atom sandwiched between two planar borazene rings with B facing N (see Fig. 1). The B–N, B–Mn, and N–Mn bond lengths are 1.45, 2.59, and 2.44 Å in $Mn(B_3N_3H_6)_2^+$, with two borazene planes separated by 3.23 Å. The magnetic moment of $4\mu_B$ is localized at the Mn site. To examine the effect of on-site Coulomb repulsion on the magnetic moment we repeated our calculation with Hubbard U ranging from 2 to 5 eV. The magnetic moment of Mn in the $Mn(B_3N_3H_6)_2^+$ cation and $Mn(B_3N_3H_6)_2$ neutral cluster remained at $4\mu_B$ and $3\mu_B$, respectively, independent of the value of U adopted. More information is given in the ESI.†

The HOMO–LUMO gap of $Mn(B_3N_3H_6)_2^+$ is 6.79 eV which is a consequence of the 18-electron shell closure rule and confirms the stability of the cation. The HOMO reflects a π bonding character and is more delocalized on the B–N dimers. Details of electron configuration are given in ESI text 1.† The ionization potential of $Mn(B_3N_3H_6)_2$, namely, 4.35 eV (see Table 1), shows that it is a super-alkali. To examine the thermal stability of $Mn(B_3N_3H_6)_2^+$ we carried out AIMD simulations at 800 K for 10 ps with ten thousand steps. The fluctuation of the total potential energy during the simulation time is given in Fig. S1b.† The average value of the total potential energy remains nearly constant during the entire time scale, confirming that the $Mn(B_3N_3H_6)_2^+$ super-alkali is stable at high temperature. By observing the simulated IR spectra, we found that the vibrational frequency distributions of $Mn(B_3N_3H_6)_2^+$ are in the 430, 970, 1400, 2700, and 3600 cm^{-1} regions. There are only three main peaks in the 890, 2700, and 3600 cm^{-1} regions of Raman spectra as shown in Fig. S2b.†

Wade–Mingos rule. The poly skeletal electron pairing theory (PSEPT) was developed by Wade[24,25] and Mingos[26,27] to account for the stability of boron-based electron deficient compounds such as boranes. The rule states that $(2n + 1)$ pairs of electrons are needed to stabilize *closo*-boranes ($B_nH_n^{2-}$) where n is the number of vertices in the boron polyhedron. Consider, for example, $B_{12}H_{12}^{2-}$. The geometry of this moiety is an icosahedron with 12 vertices occupied by 12 B atoms. The 12 H atoms are radially bonded to these B atoms. With four electrons contributed by each BH pair, there are a total of 48 electrons in $B_{12}H_{12}$. Of these 24 electrons are occupied forming the 12 BH covalent bonds, leaving behind 24 electrons to contribute to cage bonding. However, according to the Wade–Mingos rule 50 − 24 = 26 electrons are needed for cage bonding. Thus, $B_{12}H_{12}$ is stable only as a dianion.

Pathak *et al.*[6] used the Wade–Mingos rule to design a superhalogen. They accomplished this by replacing one of the B atoms in *closo*-borane with a C atom. Thus, $CB_{n-1}H_n$ would need only one electron to stabilize the molecule. The authors showed that the electron affinity of $CB_{11}H_{12}$ is 5.39 eV,[6] thus confirming that it is indeed a superhalogen.

We have explored the possibility that the Wade–Mingos rule can also be used to design a superalkali. Thus, we looked for a molecule that would have one electron more than needed to satisfy the Wade–Mingos rule. We considered $B_9C_3H_{12}$ formed by replacing three B atoms in $B_{12}H_{12}$ with C atoms. The $B_9C_3H_{12}$ moiety has a total of 51 electrons ($9 \times 3 + 3 \times 4 + 12 \times 1$), one more than $(2n + 1)$ pairs of electrons needed for the Wade–Mingos shell closure rule. Thus, $B_9C_3H_{12}^+$ should be a stable molecule. We optimized the geometry of $B_9C_3H_{12}$ by examining different isomers (see Fig. S5†). The lowest energy structure is given in Fig. 1 where carbon atoms occupy (1, 7, 9) sites in $B_9C_3H_{12}^+$. The stable $B_9C_3H_{12}^+$ structure possesses a C_{3v} symmetry with a *closo*-dodecaborate structure which is similar to the $B_{12}H_{12}^{2-}$ structure[28] shown in Fig. 1. The B–B and B–C bond lengths are around 1.79 and 1.72 Å in the $B_9C_3H_{12}^+$ cation (quite close to the 1.78 Å B–B bond length in the $B_{12}H_{12}^{2-}$ structure[28]).

The calculated ionization potential of B_9C_3H is 3.64 eV (Table 1) which confirms that it is a superalkali. The thermal stability of $B_9C_3H_{12}^+$ is confirmed by AIMD, with the Nosé heat bath scheme at 800 K for 10 ps, as shown in Fig. S1c.† No distortion or reconstruction of the boron cage is found, and the average total potential energy remains nearly constant. We found that the simulated vibrational frequencies of $B_9C_3H_{12}^+$ are at 870, 1100, 1230, 2700, and 3200 cm^{-1} of IR modes and 870, 2700, and 3300 cm^{-1} regions of Raman modes, respectively, as shown in Fig. S2c.†

By analyzing the FMOs in Fig. S3c† we see that the HOMO is more delocalized on the cage skeleton while the LUMO is localized on C and H, with a HOMO–LUMO gap of 14.77 eV. Details of electron configuration are given in ESI text 2.†

Hückel's rule. The stability of aromatic molecules is governed by Hückel's rule which requires $(4n + 2)$ electrons for a molecule to be aromatic. A classic example of an aromatic molecule is benzene (C_6H_6) which contains 6 π electrons. Here $n = 1$. To see if an organic molecule mimicking an alkali atom can be designed using Hückel's rule, we consider pyridine-H^+ ($C_5NH_6^+$) (see Fig. 1) where a tetravalent C atom is replaced by a pentavalent N atom. Thus, C_5NH_6 contains 7 π electrons, one more than needed to satisfy Hückel's rule. The geometry of the stable $C_5NH_6^+$ cation has a planar hexagonal configuration

with a C_{2v} symmetry and all carbon and nitrogen atoms contribute one p electron each to the delocalized π orbital. The C–C and C–N bond lengths of ($C_5NH_6^+$) are 1.41 and 1.37 Å, respectively. In order to confirm the stability and aromaticity of $C_5NH_6^+$ we calculated the nucleus-independent chemical shift (NICS) as well as the electron localization function (ELF). With NICS(0) and NICS(1) values at −7.78 and −9.34, respectively, and a delocalized π character we see that $C_5NH_6^+$ is aromatic. The details of our calculations are given in ESI texts 3 and 4.†

The ionization potential of C_5NH_6 is 3.95 eV, confirming that it is a superalkali (see Table 1). To further confirm the thermodynamic stability of pyridine-H^+, we followed the same method and criteria as for other systems. The temperature and potential energy plots corresponding to the initial and final snapshots are given in Fig. S1d,† which confirm its stability. The IR vibrational frequency distributions of pyridine-H^+ are located at 600, 1600, and 3500 cm^{-1}, and Raman frequencies are located at 1000 and 3200 cm^{-1}, as shown in Fig. S2d.†

The HOMO–LUMO gap of $C_5NH_6^+$ is 11.65 eV with the HOMO residing at the C–C π bonding orbital and the LUMO is located at the C and N p_z anti-bonding orbitals as shown in Fig. S3d.† Results of the electron configuration are given in ESI text 5.†

Role of superalkalis in CO_2 activation

Carbon dioxide, a major contributor to global warming, is a covalently bonded linear molecule in which carbon exists in its highest oxidation state. To convert CO_2 into fuel, catalysts are needed to first activate CO_2, *i.e.* it must transform from the linear to a bent structure. This can be accomplished by adding an electron as CO_2^- is known to have a bent geometry.[29] However, with an electron affinity of −0.6 eV CO_2^- is metastable. Thus, studies of CO_2 activation have focused on anionic complexes involving CO_2 and various atoms and molecules.

In a recent work, Bowen and coworkers[20] carried out a combined photoelectron spectroscopy and computational study of $(M–CO_2)^-$ anions (M = Cu, Ag, Au). They found that while $(Ag–CO_2)^-$ and $(Cu–CO_2)^-$ exist only in the physisorbed and chemisorbed states, respectively, $(Au-CO_2)^-$ exists in both physisorbed and chemisorbed states. Since CO_2 would assume a bent structure when an electron is transferred to it or due to its interaction with the electrons of the metal atom,[29] one would expect that the stable geometry of $(M–CO_2)^-$ would depend upon the ionization potential of the metal atom, M; an atom with a smaller ionization potential should be able to transfer an electron to CO_2 more easily than one with a large ionization potential. Similarly, the Coulomb repulsion from the metal atom would also bend the linear CO_2 structure.[29]

To see if this intuitive idea is borne out by actual calculation, we present in Fig. 2 the geometry of (a) CO_2 and (b) CO_2^-. Neutral CO_2 is a linear molecule with a C–O bond of 1.20 Å. CO_2^-, on the other hand, is a bent structure with an O–C–O bond angle of 137° and a stretched C–O bond of 1.24 Å. The electron configuration of C and O in CO_2 is $2s^{0.91}2p^{1.99}$ and $2s^{1.79}2p^{4.73}$. Once an electron is transferred, CO_2^- develops

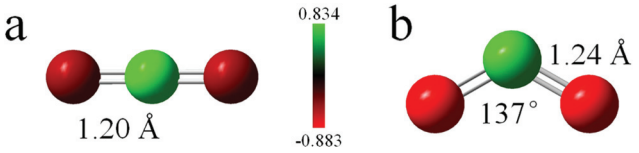

Fig. 2 Optimized geometries with bond angles and CO bond distances, and the NBO charge distribution in (a) neutral CO_2 and (b) CO_2^- anion.

a magnetic moment of $1\mu_B$ and the α-spin and β-spin of C electron configurations are $2s^{0.61}2p^{1.36}$ and $2s^{0.88}2p^{2.62}$ and O electron configurations are $2s^{0.37}2p^{0.90}$ and $2s^{0.88}2p^{2.48}$, respectively. The carbon atoms are sp hybridized in CO_2 and become quasi-sp^2 hybridized in CO_2^-, resulting in a bent structure.

We note that the ionization potentials of Cu, Ag, and Au, are, respectively, 7.73 eV, 7.58 eV, and 9.23 eV. Bowen and coworkers found the calculated O–C–O angles of $(Cu–CO_2)^-$ and $(Au-CO_2)^-$ to be 139.7° and 145.0°, respectively, while the geometry of CO_2 in $(Ag–CO_2)^-$ remained linear. However, one would have expected it to be a bent structure as in the case of $(Cu–CO_2)^-$ because both Cu and Ag have nearly the same ionization potential. These counter-intuitive results suggest that both the electronic structure and the size of the metal atom play a role in electron transfer.

As seen above, the ionization potentials of superalkalis are less than those of alkali atoms and their rational design using different electron counting rules implies that they have different electronic structures. Thus, a systematic study of the interaction of these superalkalis with CO_2 can shed light on the relative role ionization potential and the underlying electronic structure of species play on CO_2 activation. In the following we discuss these results.

Jellium rule. We study the interaction of Al_3 with CO_2. In neutral Al_3, its HOMO has a large density distribution around Al atoms in the triangle plane as in Fig. S4a,† which would make CO_2 prefer to adsorb at the position where the charge density is maximum. In the stable configuration as shown in Fig. 3a, the distance between CO_2^- and Al_3^+ is 1.95 Å, the O–C

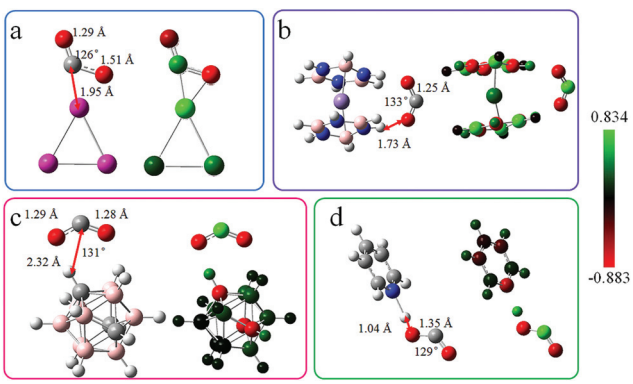

Fig. 3 (a) to (d) Optimized geometries (left panel) and NBO charge distribution (right panel) of four different kinds of neutral superalkalis interacting with the CO_2 molecule.

bonds extend to 1.29 and 1.51 Å, about 4.4%–22% longer than that in the CO_2 anion. This bond stretching is the result of bond weakening, making it easier to activate the CO_2 molecule. The corresponding O–C–O angle in Al_3CO_2 is 126° making the bond-bending 8% larger than the corresponding value in CO_2^-. This is consistent with the amount of charge transfer. Natural bond orbital (NBO) analysis in Fig. 3a shows that 1.26*e* charge is transferred from Al_3 to CO_2 (see Table 1) which is larger than that in a noble metal atom (0.77*e*),[30] and the CO_2 anion (1*e*).

In neutral Al_3 the α-spin and β-spin electron configurations of Al are $3s^{0.78}3p^{0.87}$ and $3s^{0.61}3p^{0.72}$, respectively. When the CO_2 is adsorbed, the α-spin and β-spin electron configurations of Al change to $3s^{0.78}3p^{0.66}$ and $3s^{0.79}3p^{0.33}$ in Al_3 and that of C and O are $2s^{0.55}2p^{1.22}$ and $2s^{0.89}2p^{2.53}$; $2s^{0.54}2p^{1.21}$ and $2s^{0.89}2p^{2.53}$ in CO_2. The electron gain of 0.57*e* in the α-spin and 0.59*e* in the β-spin configurations results in the bending of CO_2.

18-Electron rule. Here we study the interaction between $Mn(B_3N_3H_6)_2$ and CO_2. The corresponding geometry is given in Fig. 3b. Note that the O atom of CO_2 is bound to the H atom that is attached to N. The distance between CO_2 and $Mn(B_3N_3H_6)_2$ is 1.73 Å. Both the O–C bonds are extended to 1.25 Å which is slightly longer than that of 1.24 Å in CO_2^-. The O–C–O angle in $Mn(B_3N_3H_6)_2CO_2$ is 133° indicating that the bending of CO_2 interacting with this superalkali is 3% more than that in CO_2^-. NBO analysis in Fig. 3b shows that 0.90*e* charge is transferred from $Mn(B_3N_3H_6)_2$ to CO_2 (see Table 1). More details of this calculation are given in ESI texts 6 and 7.†

Wade–Mingos rule. The geometry of $B_9C_3H_{12}CO_2$ following the interaction of CO_2 with $B_9C_3H_{12}$ is shown in Fig. 3c. In the $B_9C_3H_{12}$ neutral cluster, the HOMO has a large electron density distribution around carbon atoms in the triangle plane (Fig. S4c†) where CO_2 prefers to bind. In this configuration the distance between CO_2 and $B_9C_3H_{12}$ is 2.32 Å with the O–C bonds are extended to 1.29 and 1.28 Å. These are about 3.3%–4.4% longer than that in CO_2^-. In addition, the O–C–O angle is 131° resulting in a structure that is 4% more bent than CO_2^-. Thus, both the stretching of the O–C bonds and the bending of the O–C–O angle weaken the O–C bonds of CO_2, making it easy to activate.

NBO analysis in Fig. 3c and Table 1 shows that, after CO_2 adsorption, the total charge transferred from $B_9C_3H_{12}$ to CO_2 is about 0.912*e*, which is more than that in noble metal atoms (0.77*e*).[30] In addition, the CO_2 α-spin electron configuration gains 0.89*e* (details are given in ESI texts 8 and 9†) making carbon more sp^2 hybridized and causing CO_2 to bend (see Fig. 3c).

Hückel's rule. The geometry of C_5NH_6 interacting with CO_2 is shown in Fig. 3d. In the stable configuration, the distance between CO_2 and C_5NH_6 is 1.04 Å. The O–C bonds are extended to 1.35 Å which is about 9.3% longer than that in CO_2^-. In addition, the O–C–O bond angle is 129° compared to 137° in CO_2^-. Both these factors help to activate the CO_2 molecule. NBO analysis in Fig. 3d shows that 0.632*e* (details are given in ESI texts 10 and 11†) charge is transferred from C_5NH_6 to CO_2 (see Table 1). This amount of charge transfer is smaller than that in a noble metal gas (0.77*e*).[30]

Comparison between the roles played by different superalkalis

As discussed above, all superalkalis donate charge to CO_2, although to a varying degree. This charge transfer results in bending of the CO_2 molecule and weakening of the C–O bond, thus making it easier to break. Here, we compare the relationship between the ionization potential of the superalkalis, the amount of charge they transfer to CO_2, and the angle to which the CO_2 bends as a result. This will allow us to identify the dominant factor for CO_2 activation in Table 1. Comparing Al_3 and $Mn(B_3N_3H_6)_2$, whose IPs are comparable, the smaller volume of the superalkali leads to more CO_2 bending. Besides, comparing Al_3 and C_5NH_6, whose volumes are comparable, the lower the IP of superalkali, the more is the bending of CO_2. In addition, note that among all the superalkalis studied, the IP of Al_3^+ is not the lowest, the charge transferred is not the most, and the volume is not the smallest, yet it is able to bend the CO_2 molecule the most. This comparison suggests that the quantitative nature of CO_2 activation would depend upon the underlying electronic structure and size of the superalkali, although one can generally argue that the charge transfer made possible by low ionization potential is a driving factor in CO_2 activation.

Conclusions

In summary, we show that a large family of superalkalis can be designed by going beyond the current use of the octet electron counting rule. These include the jellium shell closure rule valid for clusters of nearly free electron metals, the 18-electron rule valid for clusters containing transition metal atoms, the Wade–Mingos rule valid for compounds containing electron deficient boron, and Hückel's rule valid for organic molecules. While we have only used Al_3^+, $Mn(B_3N_3H_6)_2^+$, $B_9C_3H_{12}^+$, and $C_5NH_6^+$ as examples to illustrate our rational design principle, numerous superalkalis can now be designed using these electron counting rules, thus vastly expanding the scope of superatoms that mimic the chemistry of alkali atoms. To demonstrate the use of these superalkalis in chemical applications, we focused on CO_2 activation which is the first step for producing fuels from CO_2. Realizing that the addition of an extra electron results in a bent CO_2^- anion and that a superalkali with an ionization potential less than that of an alkali atom can easily transfer an electron, we studied the reaction of these superalkalis with CO_2 by computing their equilibrium geometry and charge distribution. In all cases CO_2 was found to be negatively charged, although the amount of charge transfer depends on the nature of the superalkali. In all cases, however, the O–C–O bond angle is found to be smaller than that in the gas phase CO_2^-. These results based on density functional theory suggest that superalkalis can be used as catalysts for CO_2 activation.

Theoretical methods

The atomic structure optimizations, NICS values, and vibrational frequencies (IR and Raman) are calculated at the MP2 level of theory.[31–33] Single point calculations of energy, molecular orbitals, band gaps, and NBO analysis are calculated at the CCSD level of theory,[34,35] using optimized geometries obtained at the MP2 level. We used the 6-311+G* basis set for all atoms[36] embedded in the Gaussian 09 code.[37] Frequency analysis was performed at the same level of theory to ensure that there are no imaginary frequencies and the structures belong to minima in the potential energy surface. Thermodynamic stability, magnetic properties, and ELF analysis[38] are repeated using density functional theory (DFT) as implemented in the VASP.[39] The projector augmented wave (PAW) method[40] and Perdew–Burke–Ernzerhof (PBE)[41] exchange correlation functional within the generalized gradient approximation (GGA) are used. Plane waves with a kinetic energy cutoff of 500 eV are used to expand the valence electron wave functions. For all structural relaxations the convergence criteria for total energy and Hellmann–Feynman force are set to be 10^{-4} eV and 10^{-2} eV Å^{-1}, respectively. A unit cell with a vacuum space of 30 Å in three directions is used in order to avoid virtual interactions. The first Brillouin zone is sampled by the Γ-point.[42] *Ab initio* molecular dynamics (AIMD) simulations are also performed to assess the thermal stability of different cations. A canonical (NVT) ensemble is adopted using the Nosé heat bath method.[43]

Acknowledgements

This work is partially supported by grants from the National Natural Science Foundation of China (NSFC-51471004), the National Key Research and Development Program of China (Grant No. 2016YFE0127300), and the Doctoral Program of Higher Education of China (20130001110033). P. J. acknowledges support by the U.S. Department of Energy, Office of Basic Energy Sciences, Division of Materials Sciences and Engineering under Award No. DE-FG02-96ER45579. T. Z. acknowledges the China Scholarship Council (CSC) for sponsoring his visit to Virginia Commonwealth University (VCU). Resources of the National Energy Research Scientific Computing Center are supported by the Office of Science of the U.S. Department of Energy under Contract No. DE-AC02-05CH11231.

References

1 S. N. Khanna and P. Jena, *Phys. Rev. Lett.*, 1992, **69**, 1664–1667.
2 S. N. Khanna and P. Jena, *Phys. Rev. B: Condens. Matter*, 1995, **51**, 13705–13716.
3 G. L. Gutsev and A. I. Boldyrev, *Chem. Phys. Lett.*, 1982, **92**, 262–266.
4 G. L. Gutsev and A. I. Boldyrev, *Chem. Phys.*, 1981, **56**, 277–283.
5 H.-J. Zhai, J. Li and L.-S. Wang, *J. Chem. Phys.*, 2004, **121**, 8369–8374.
6 B. Pathak, D. Samanta, R. Ahuja and P. Jena, *ChemPhysChem*, 2011, **12**, 2423–2428.
7 B. Z. Child, S. Giri, S. Gronert and P. Jena, *Chem. – Eur. J.*, 2014, **20**, 4736–4745.
8 G. L. Gutsev, B. K. Rao, P. Jena, X.-B. Wang and L.-S. Wang, *Chem. Phys. Lett.*, 1999, **312**, 598–605.
9 S. Giri, S. Behera and P. Jena, *Angew. Chem., Int. Ed.*, 2014, **53**, 13916–13919.
10 H. Fang and P. Jena, *J. Mater. Chem. A*, 2016, **4**, 4728–4737.
11 Q. Yao, H. Fang, K. Deng, E. Kan and P. Jena, *Nanoscale*, 2016, **8**, 17836–17842.
12 P. Jena, *J. Phys. Chem. Lett.*, 2015, **6**, 1549–1552.
13 P. Jena, *J. Phys. Chem. Lett.*, 2013, **4**, 1432–1442.
14 J. Tong, Y. Li, D. Wu and Z.-J. Wu, *Inorg. Chem.*, 2012, **51**, 6081–6088.
15 N. Hou, Y. Li, D. Wu and Z.-R. Li, *Chem. Phys. Lett.*, 2013, **575**, 32–35.
16 S. Giri, S. Behera and P. Jena, *J. Phys. Chem. A*, 2014, **118**, 638–645.
17 D. Wang, J. D. Graham, A. M. Buytendyk and K. H. Bowen, *J. Chem. Phys.*, 2011, **135**, 164308.
18 X. Li, H. Wu, X.-B. Wang and L.-S. Wang, *Phys. Rev. Lett.*, 1998, **81**, 1909–1912.
19 B. K. Rao and P. Jena, *J. Chem. Phys.*, 1999, **111**, 1890–1904.
20 X. Zhang, E. Lim, S. K. Kim and K. H. Bowen, *J. Chem. Phys.*, 2015, **143**, 174305.
21 P. Pyykkö and N. Runeberg, *Angew. Chem., Int. Ed.*, 2002, **41**, 2174–2176.
22 X. Li, B. Kiran, J. Li, H.-J. Zhai and L.-S. Wang, *Angew. Chem., Int. Ed.*, 2002, **41**, 4786–4789.
23 R. Pandey, B. K. Rao, P. Jena and M. A. Blanco, *J. Am. Chem. Soc.*, 2001, **123**, 3799–3808.
24 K. Wade, *J. Chem. Soc. D*, 1971, 792–793, DOI: 10.1039/C29710000792.
25 K. Wade, in *Advances in Inorganic Chemistry and Radiochemistry*, ed. H. J. Emeléus and A. G. Sharpe, Academic Press, 1976, vol. 18, pp. 1–66.
26 D. M. P. Mingos, *Acc. Chem. Res.*, 1984, **17**, 311–319.
27 D. M. P. Mingos, *Chem. Soc. Rev.*, 1986, **15**, 31–61.
28 J. A. Wunderlich and W. N. Lipscomb, *J. Am. Chem. Soc.*, 1960, **82**, 4427–4428.
29 G. L. Gutsev, R. J. Bartlett and R. N. Compton, *J. Chem. Phys.*, 1998, **108**, 6756–6762.
30 X. Zhang, G. Liu, K.-H. Meiwes-Broer, G. Ganteför and K. Bowen, *Angew. Chem., Int. Ed.*, 2016, **55**, 9644–9647.
31 M. Head-Gordon, J. A. Pople and M. J. Frisch, *Chem. Phys. Lett.*, 1988, **153**, 503–506.
32 S. Sæbø and J. Almlöf, *Chem. Phys. Lett.*, 1989, **154**, 83–89.
33 M. J. Frisch, M. Head-Gordon and J. A. Pople, *Chem. Phys. Lett.*, 1990, **166**, 275–280.
34 G. D. Purvis and R. J. Bartlett, *J. Chem. Phys.*, 1982, **76**, 1910–1918.

35 G. E. Scuseria, C. L. Janssen and H. F. Schaefer, *J. Chem. Phys.*, 1988, **89**, 7382–7387.
36 M. J. Frisch, J. A. Pople and J. S. Binkley, *J. Chem. Phys.*, 1984, **80**, 3265–3269.
37 M. Frisch, G. Trucks, H. B. Schlegel, G. Scuseria, M. Robb, J. Cheeseman, G. Scalmani, V. Barone, B. Mennucci and G. Petersson, Inc., Wallingford, CT, 2009, vol. **270**, p. 271.
38 A. D. Becke and K. E. Edgecombe, *J. Chem. Phys.*, 1990, **92**, 5397–5403.
39 G. Kresse and J. Furthmüller, *Phys. Rev. B: Condens. Matter*, 1996, **54**, 11169.
40 P. E. Blöchl, *Phys. Rev. B: Condens. Matter*, 1994, **50**, 17953–17979.
41 J. P. Perdew, K. Burke and M. Ernzerhof, *Phys. Rev. Lett.*, 1996, **77**, 3865.
42 H. J. Monkhorst and J. D. Pack, *Phys. Rev. B: Solid State*, 1976, **13**, 5188–5192.
43 S. Nosé, *J. Chem. Phys.*, 1984, **81**, 511–519.